ULTIMATE LOAD BEHAVIOUR OF BOX-COLUMNS UNDER COMBINED LOADING OF AXIAL COMPRESSION AND TORSION

M.MAHENDRAN and N.W.MURRAY†,

Dept. of Civil Engineering, Monash University,

Clayton, Victoria 3168, Australia.

ABSTRACT

This paper describes a study of the theoretical and experimental behaviour of box-columns of varying b/t ratios under loadings of axial compression and torsion and their combinations. Details of the testing rigs and the testing methods, the results obtained such as the load-deflection curves and the interaction diagrams, and many experimental observations regarding the behaviour of box-models and the types of local plastic mechanisms associated with each type of loading are presented. A simplified rigid-plastic analysis is carried out to study the collapse behaviour of box-columns under these loadings, based on the observed plastic mechanisms and the results are compared with those of experiments.

1. INTRODUCTION

One of the commonest thin-walled structure is a box-section which has been utilised widely in large columns, bridges and for members in stationary and moving industrial structures. When box-sections are used as parts of the structure, they are not always subjected to axial compression only, but to combined loading of axial compression, torsion and bending. The behaviour of box-sections under axial compression is fairly well-understood, but this is not so when they are subjected to loadings accompanied by torsion. The ultimate load of box-sections, even when they carry only torsional loading, cannot be predicted. Scheer and Nölke[1] have shown that it would be extremely dangerous to use the plate girder theories for box-sections. However, their test results revealed that it is satisfactory to design

† Author to whom correspondence should be addressed

box-sections using the German code specifications[2] which are based on linear theories. But, reliance on an elastic analysis and first yield as the limiting criterion could result in an unnecessarily conservative design. The investigation described here has therefore been carried out to find out how box-sections respond to axial, torsional and combined axial-torsional loading.

2. EXPERIMENTAL ANALYSIS

2.1 GENERAL

Fifty-four small-scale steel square box-specimens of width/thickness ratios (b/t) of 60, 78, 100 and 158 were tested with various combinations of axial compression and torsion. The tests with single loadings were completed first and these were followed by those with combined loading. Some box-specimens of high b/t ratios of 200 and 300 were also tested in single loadings in order to obtain a complete ultimate-strength diagram. In order to fabricate box-specimens of different b/t ratios, only the thickness (t) was changed. Except for five longer box-specimens (length/width L/b = 9), all had a constant L/b ratio of 4.3. The specimen length, chosen to represent the part between two adjacent rigid diaphragms, ensured that the central regions of the box-specimen would deform without any restraint from the loaded edges which had complete rotational fixity. The ends of all the test specimens were strengthened by means of a layer of plaster in order to prevent any premature localized buckling.

Fig.1 shows the cross-sectional dimensions of a typical specimen and the method of fabrication. A simpler method of seam-welding was chosen in order to minimize the initial imperfections and residual stresses. This method of fabrication was the same as that used by Scheer and Nölke[1], Scheer et al.[3], and Lacher and Böhm[4]. There would be some effects on the behaviour due to the projections in the specimen, but Scheer and Nölke's[1] experiments

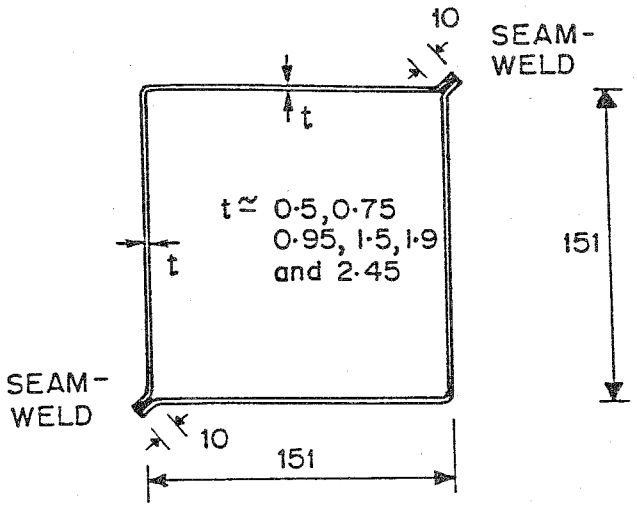

FIGURE 1 Cross-sectional Dimensions of A Typical Box-Specimen

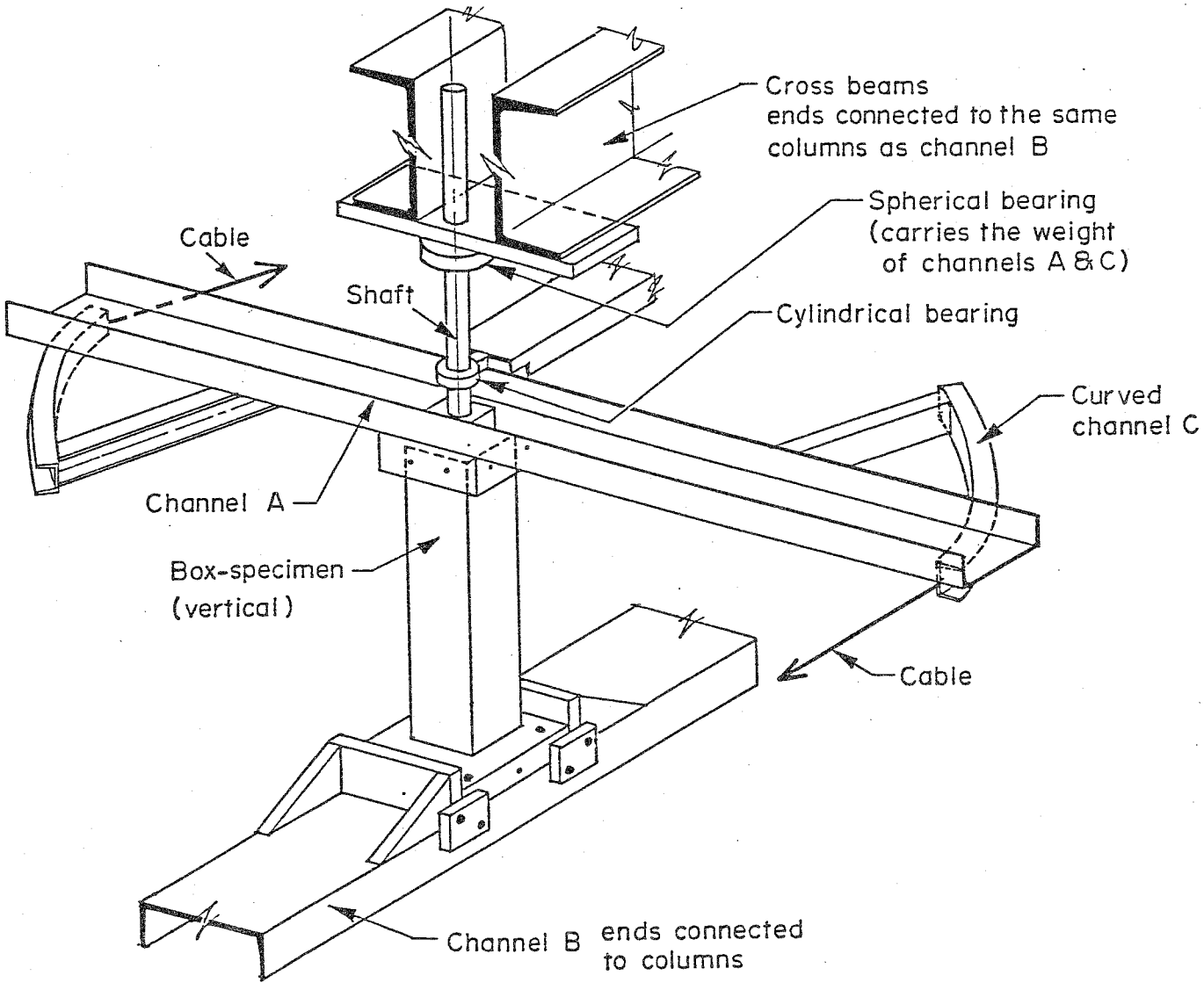

FIGURE 2 A Simple Isometric View of the Torsion Testing Rig

on torsion confirmed that the type of joints used in fabricating the box-specimens did not have much influence on the collapse loads or the behaviour. Theoretical considerations showed that in the present programme the small projections would have had only a small influence upon either the torsional or axial properties of the specimens. The yield and ultimate stresses of steel were in the range of 195 to 245 MPa and 310 to 340 MPa, respectively for thicker sheets (1.90 and 2.45 mm), and 260 to 310 MPa and 340 to 375 MPa, respectively for thinner sheets.

2.2 TESTS WITH AXIAL COMPRESSION

Altogether nine axial compression tests were performed in an ordinary testing machine. The Moire fringe technique was used to obtain contour maps of the out-of-plane deflection in all categories of test.

2.3 TESTS WITH TORSION

Altogether sixteen tests were carried out with pure torsion. An isometric view of the rotating component of the testing rig and an aerial view of the entire testing rig are given in Fig.2 and Plate 1, respectively. An important component of the testing rig was the rotating channel A which was a 254x89x36 section of length 3500 mm and was hung from the cross-beams by means of a spherical bearing. Another cylindrical type of bearing was also installed to stabilize the rotating component. The height of channel A could be changed easily by readjusting the spherical bearing if it was required to accommodate shorter or longer specimens. The box-specimen with cover plates at the top and bottom was placed within the space between the channel A and the fixed channel B. Channel A was rotated by pulling the cables each of 12 mm diameter at the ends in opposite directions around two small curved channels C at a distance of 1525 mm from the axis of the shaft. The radii of the curved channels C were also set equal to the distance of 1525 mm. Plate 2 shows the special arrangement by which channel A was pulled by means of hydraulic jacks via the cables. Altogether four

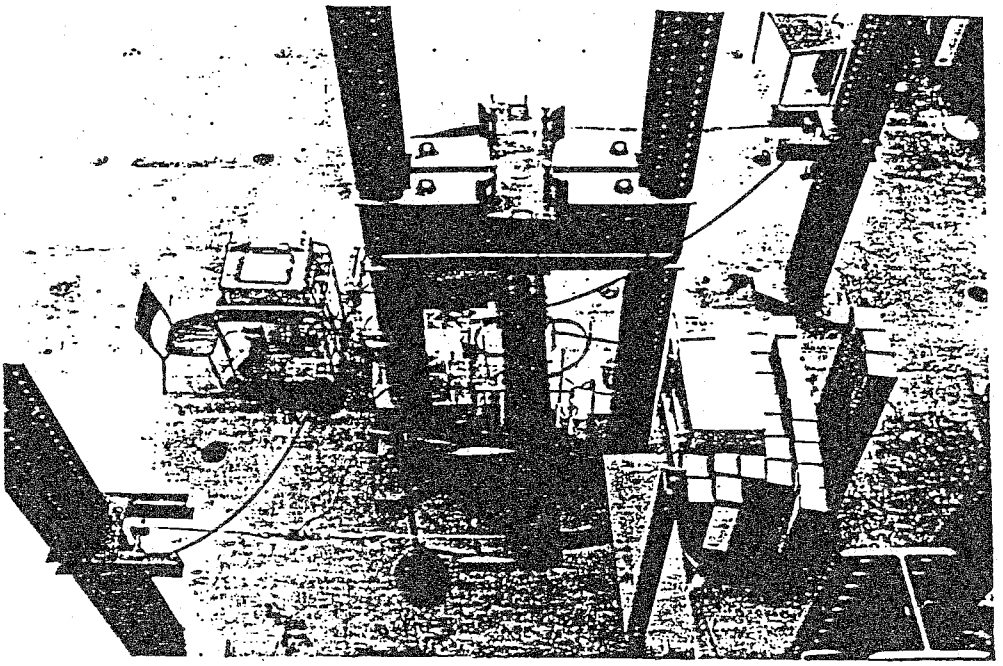

PLATE 1 An Aerial View of the Torsion Testing Rig

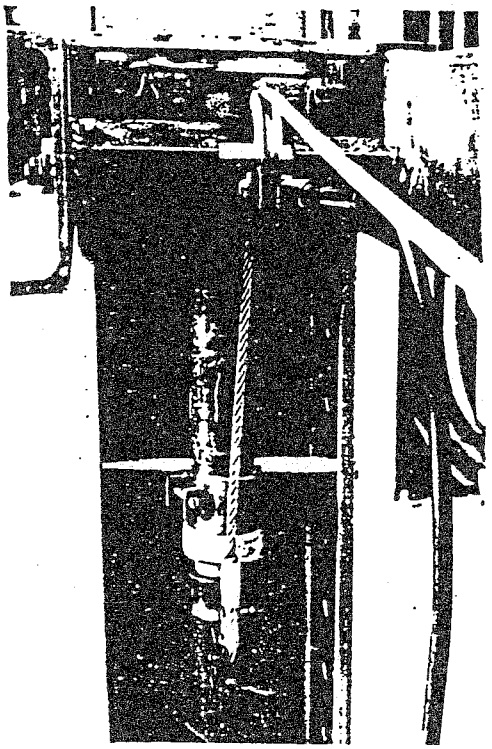

Hydraulic Jack - Pulley Arrangement

PLATE 2 Components of the Torsion Testing Rig

universal columns were used in the testing rig, two of which were used in the above hydraulic jack-pulley arrangement and the other two were used for fixing the bottom channel B and the cross-beams.

The tensile force in each of the two cables was measured by a tension load cell which was fixed to the cable midway between the pulley and channel C. The tensile forces in the cables were maintained equal by monitoring through the display on the exciter connected to each load cell and the rotation of the specimen was measured at the ends of two sets of long bars fixed around the plastered parts of the specimens via displacement transducers. All displacement transducers and load cells were connected to a datalogger which printed out the readings.

2.4 TESTS WITH COMBINED AXIAL COMPRESSION AND TORSION

Altogether 29 tests were carried out with combined loading. Five longer specimens were used in the case of loadings with a small axial load component in order to accommodate the steeply-spiralling mechanisms on all four sides. The specimen was loaded first with an axial compression force up to a predetermined value between zero and the ultimate capacity of the specimen in pure axial compression, and then loaded with torsion to failure while maintaining the constant axial compression force. In practice, this loading sequence is more likely than that in the reverse order because, for example, a loaded crane would have axial compression in one of its members and, during slewing operations or during a wind gust, torsion could be introduced.

The torsion testing rig was modified in order to load the specimen with combined axial compression and torsion, each of which could be carried out independently. Fig.3 shows the details of the modified components of the testing rig. Additional components, namely a hydraulic jack, a load cell and a loading plate were accommodated in the space between the bottom

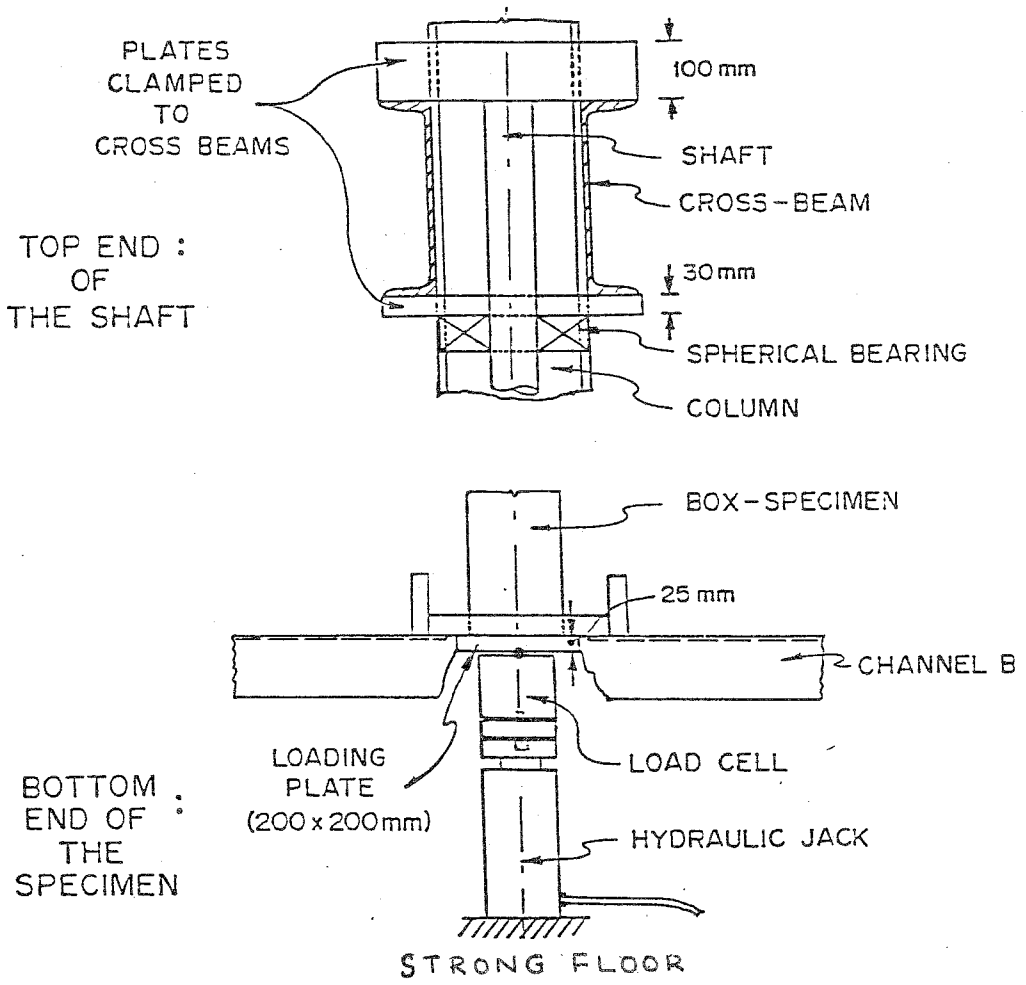

FIGURE 3 Additional Components used in Tests with Combined Loading

channel B and the strong floor. A hole was cut through the channel B to allow axial loading of the specimen. The bottom cover plate of the specimen was no longer bolted to the channel B, but it was free to move vertically. The top-end of the shaft was prevented from moving by means of a very heavy plate of thickness 100 mm clamped to the cross-beams.

3. EXPERIMENTAL RESULTS

3.1 TESTS WITH AXIAL COMPRESSION

The box-specimens of low b/t ratios (60 and 78) developed roof shaped mechanisms (Plate 3) and those of high b/t ratios developed the so-called flip-disc mechanisms (Plate 4) at the same level on all four sides with alternating concavity and convexity. In general, the behaviour of box-specimens fell into two groups depending on these types of mechanism. Fig.4 presents the curve of ultimate strength in axial compression σ_{pu} versus plate slenderness factor $\bar{\lambda}$ ($=\sqrt{\frac{\sigma_f}{\sigma_{cr}}}$) recommended by some code specifications where σ_f and σ_{cr} are the yield stress and the plate buckling stress in axial compression, respectively. All experimental results are plotted in the same figure and they exhibit a sufficient margin of safety when compared with the curve of allowable stress (safety factor $\gamma = 1.5$) recommended by the German code[2]. However, experimental results belonging to thinner box-columns appeared to have a greater margin of safety than that of thicker box-columns, due to the available post-buckling strength of thinner box-columns which is ignored by the linear buckling theory adopted by the codes.

3.2 TESTS WITH TORSION

In general, the behaviour of box-specimens again fell into two groups as in the tests with axial compression. The specimens developed similarly shaped mechanisms, but they were inclined at approximately 30^o to the axis of the box-specimen and not at a right angle as in the tests with axial compression

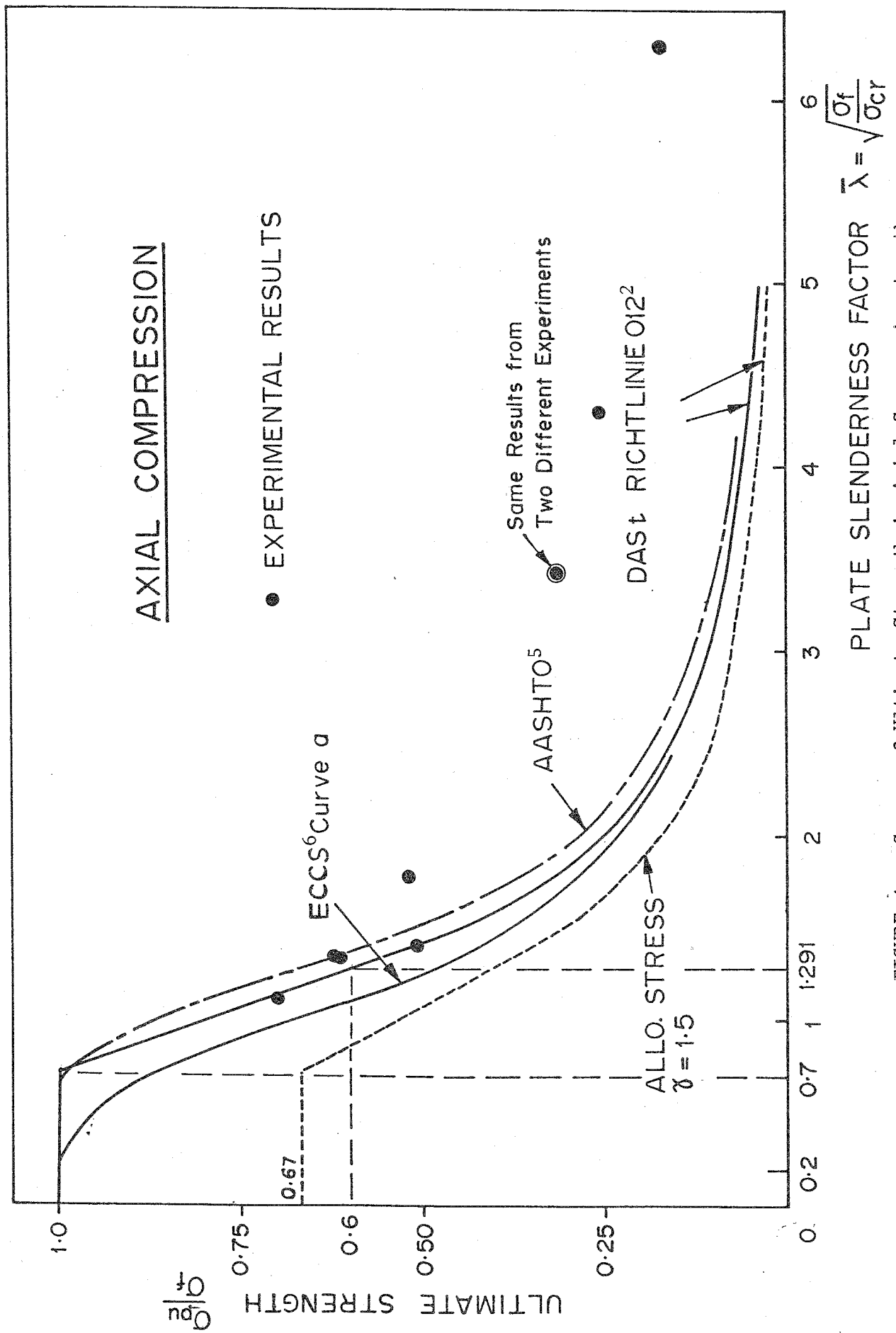

FIGURE 4 Curves of Ultimate Strength in Axial Compression together with Experimental Results

(Plates 3 and 4). Tests showed that the presence of a spiralling mechanism in only two sides was sufficient to fail the box-specimen in pure torsion. This result is similar to that found by Murray and Lau[7] in their tests on channel cantilevers. Fig.5 compares the experimental results with the curves of ultimate strength in shear (τ_{pu}) versus plate slenderness factor $\bar{\lambda}$ ($=\sqrt{\frac{\tau_f}{\tau_{cr}}}$) according to plate girder theories developed by Basler[8], Höglund[9] and Herzog[10], and those recommended by some code specifications, where τ_f and τ_{cr} are the shear yield stress equal to $\frac{\sigma_f}{\sqrt{3}}$ and the plate shear buckling stress, respectively. The experimental ultimate strength values obtained here appear to agree with those obtained from Scheer and Nölke's[1] experiments (Fig.5). As observed by Scheer and Nölke[1], plate girder theories were found to overestimate the ultimate strength of box-columns in torsion in the present case also. However, Basler's[8] theory is safer to use for box-columns of high b/t ratios ($\bar{\lambda} > 1.5$, see Fig.5). The German code[2] recommends the same curve for shear and axial compressive loadings in this non-dimensionalized format, but with a smaller safety factor γ of 1.32 for the former. Comparison of experimental results with this curve leads to the same comments made in the case of axial compression.

The presence of initial imperfections and residual stresses did not seem to have a significant effect on box-columns in torsion. A different method of fabrication such as arc-welding along all four corners of the box-section, which would have increased the magnitude of such imperfections, was used in some box-specimens, but the decrease in the ultimate strength of the specimens was insignificant. This observation is similar to those made in the past about the shear behaviour of plates by Harding et al.[11], Dowling et al.[12] and Massonnet and Janss[13], and the torsional behaviour of box-sections by Scheer and Nölke[1].

3.3 TESTS WITH COMBINED LOADING

The behaviour of box-specimens under combined loading was again of two types. They still developed similarly-shaped plastic mechanisms as before. The mechanism which formed perpendicular to the axis of the specimen under pure axial compression and at approximately 30^{o} under pure torsion was inclined at angles between these two values when the specimen was tested with combined axial compression and torsion. Plates 3 and 4 show that as the applied axial compression component in combined loading was decreased and the torque increased, the axis of the mechanisms became more elongated. The same effects are also indicated by the corresponding Moire fringe photographs of the two types of mechanisms obtained during the tests (Plates 5 and 6). The mechanisms spiralled around the specimen as in the tests with torsion, but all four sides failed in this case.

The ultimate torsional moment, the ductility and the post-collapse strength of the specimen decreased as the axial compression component in combined loading was increased. In the tests conducted with large axial compression closer to the ultimate capacity of the specimen in pure axial compression, the specimen collapsed rapidly from its ultimate torsional moment and pre-set axial compression. Longer specimens behaved in a similar manner to shorter ones tested with the same loading and were able to accommodate the long spiralling mechanisms on all four sides.

Some specimens developed a combined elastic buckling mode under the action of torsion and axial compression. This buckling mode appeared to fall between those in pure axial compression and in pure torsion (Plate 7(b)) and are in agreement with the plots obtained using a finite strip buckling analysis[14].

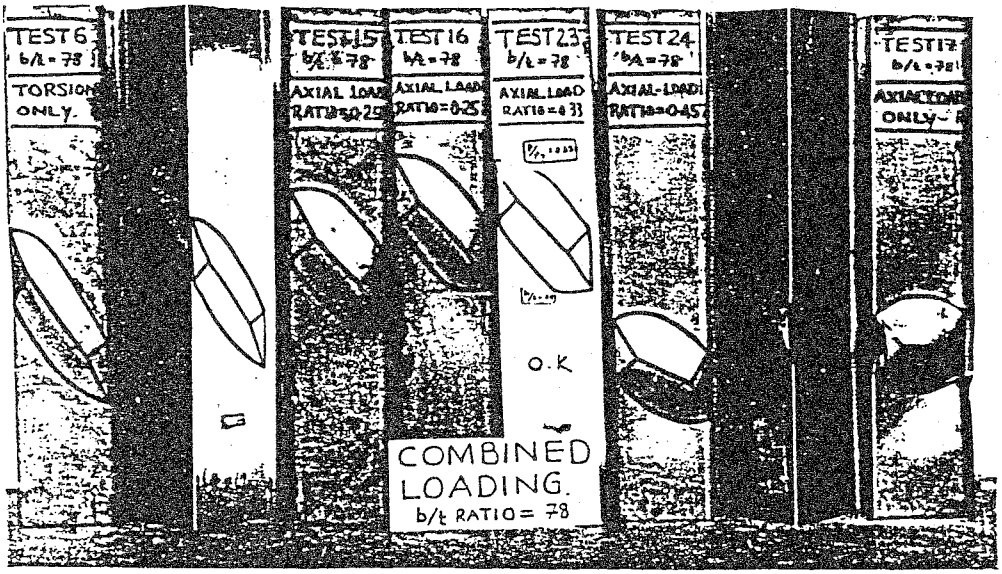

PLATE 3 Box-specimens of b/t Ratio = 78 after Failure in Combined Loading of Axial Compression and Torsion - Roof Mechanism

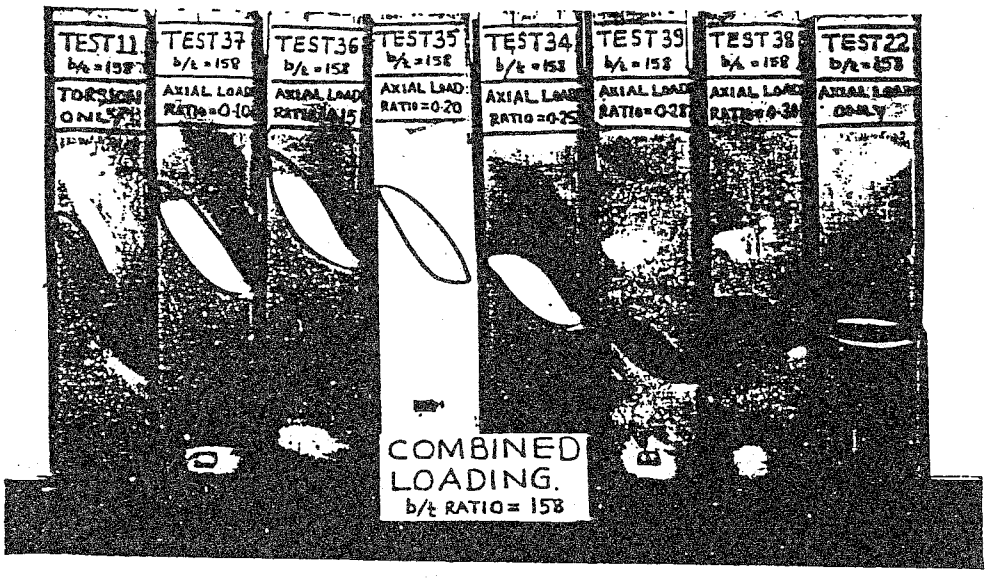

PLATE 4 Box-specimens of b/t Ratio = 158 after Failure in Combined Loading of Axial Compression and Torsion - Flip-disc Mechanism

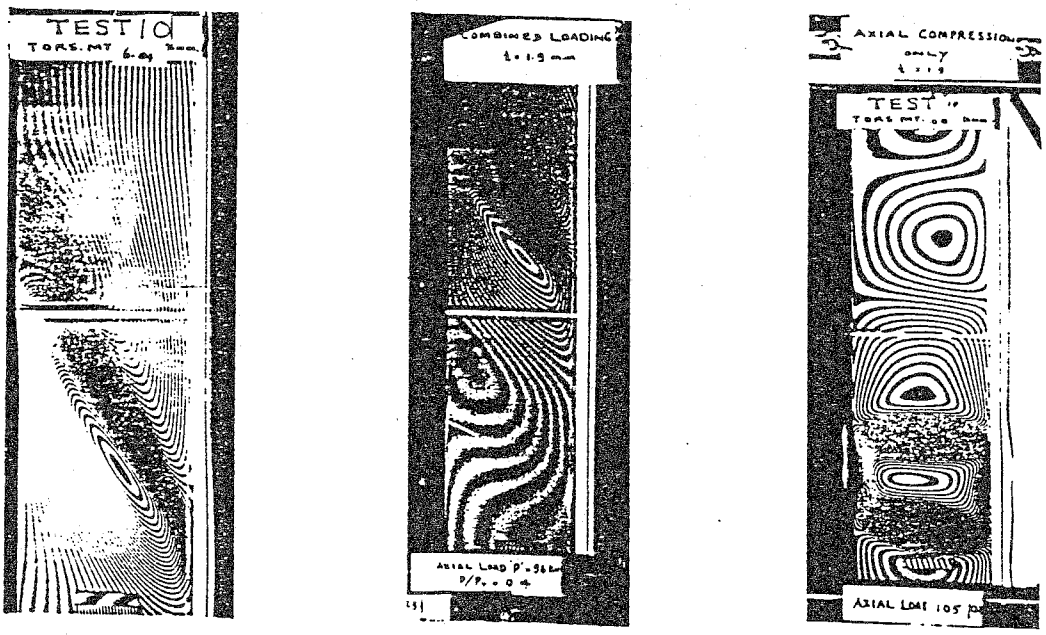

(a).Torsion only (b).Combined Loading (c).Axial Compression only

PLATE 5 Moire Fringe Patterns of Roof Mechanisms

- Box-specimens of b/t Ratio = 78

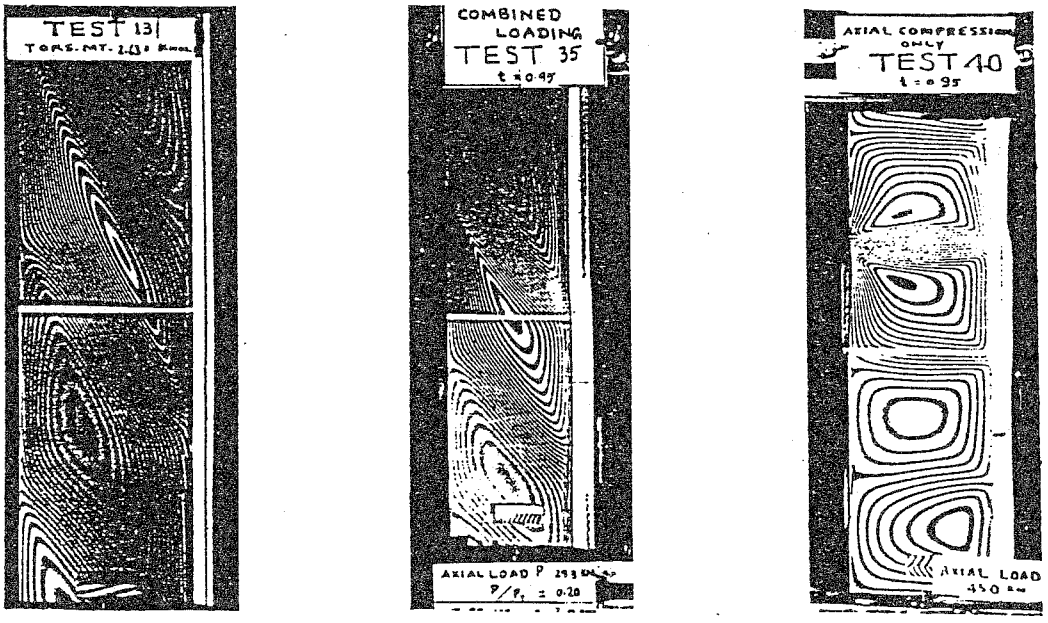

(a).Torsion only (b).Combined Loading (c).Axial Compression only

PLATE 6 Moire Fringe Patterns of Flip-disc Mechanisms

- Box-specimens of b/t Ratio = 158

In all categories of test, thicker specimens which developed roof mechanisms collapsed in a ductile manner compared with thinner specimens which developed flip-disc mechanisms. This is because in the former case there are significant regions which undergo in-plane yielding, i.e., failure is by developing a quasi-mechanism[15].

3.4 INTERACTION DIAGRAMS

Fig.6 is an interaction diagram of ultimate shear stress ($\frac{\tau_u}{\tau_f}$) versus maximum (applied) axial compressive stress ($\frac{\sigma_a}{\sigma_f}$) in a non-dimensionalized form. The interaction diagrams of box-columns with b/t ratios of 60 and 78 appear to be similar to each other and the same is true with b/t ratios of 100 and 158. In the case of thicker box-columns the increasing magnitude of axial compression component in combined loading gradually reduced the carrying capacity of the box-column in torsion (Fig.6) whereas in the case of thinner box-columns, the torsional strength suddenly decreased to zero as the axial compression approached the ultimate capacity of the box-column in pure axial compression. When the interaction diagrams are presented in a different format (Fig.7), the graph represented by the following equation

$$\left(\frac{\sigma_a}{\sigma_{pu}}\right) + \left(\frac{\tau_u}{\tau_{pu}}\right)^2 = 1 \qquad \ldots(1)$$

is the best-plot suitable in the case of thicker box-columns (b/t=60 and 78). For thinner box-columns, the graphs represented by the following equations,

$$\left(\frac{\sigma_a}{\sigma_{pu}}\right) + \left(\frac{\tau_u}{\tau_{pu}}\right)^{9/2} = 1 \qquad \ldots(2a)$$

$$\left(\frac{\sigma_a}{\sigma_{pu}}\right) + \left(\frac{\tau_u}{\sigma_{pu}}\right)^{10} = 1 \qquad \ldots(2b)$$

prove to be the best-plots for b/t ratios of 100 and 158, respectively.

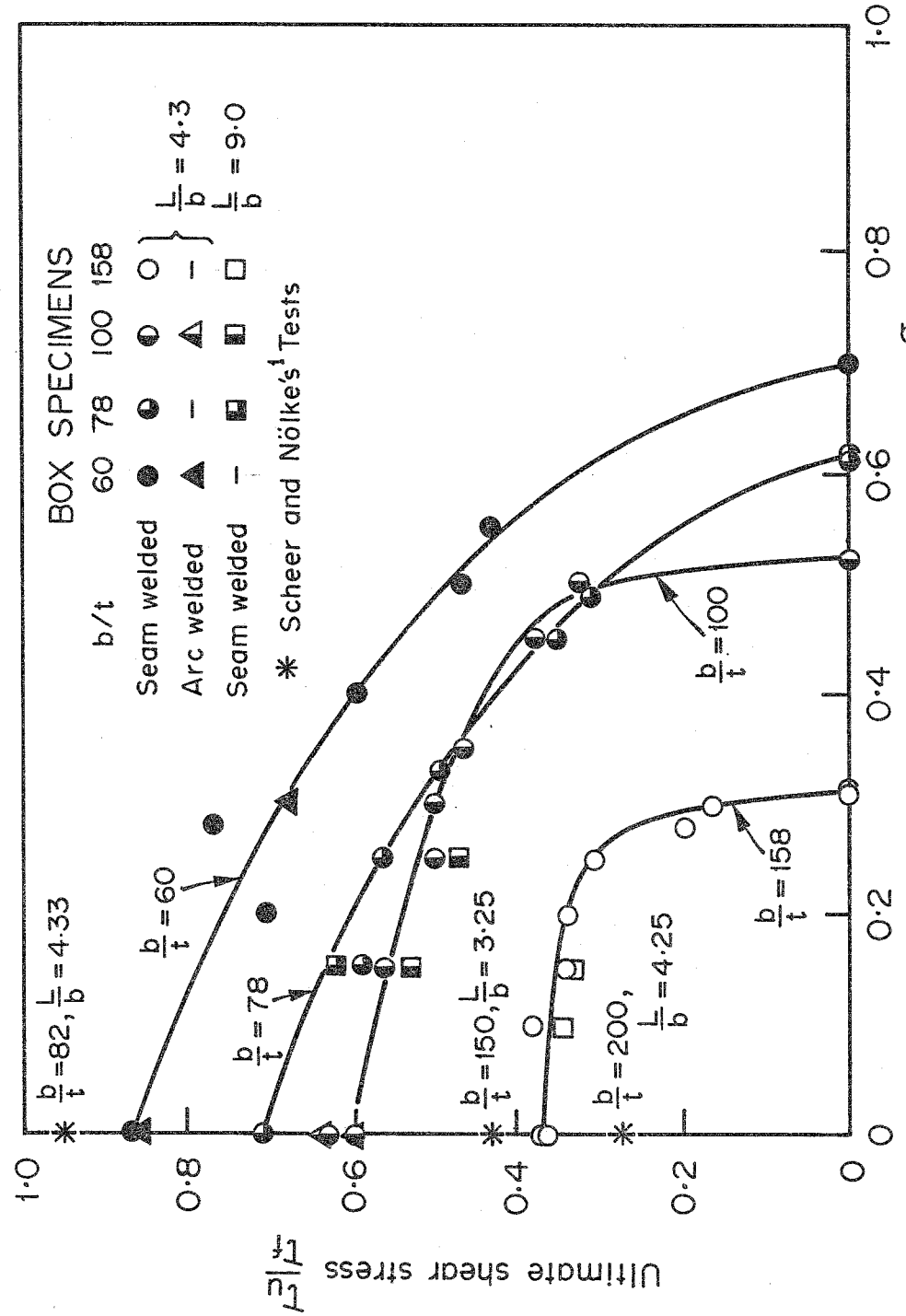

FIGURE 6 Experimental Interaction Diagrams for Box-columns

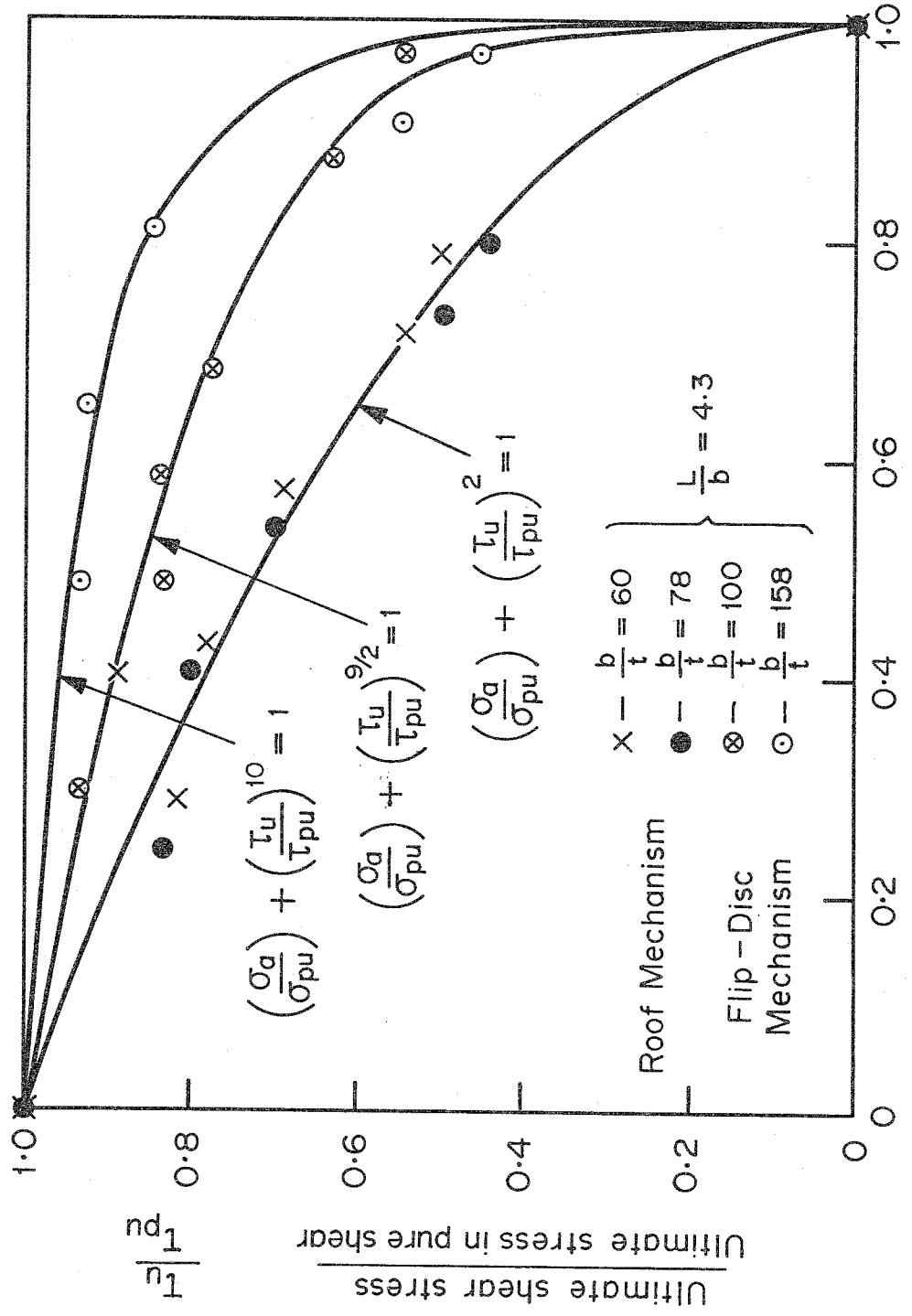

FIGURE 7 Experimental Interaction Diagrams for box-columns of b/t Ratios = 60, 78, 100 and 158

4. RIGID-PLASTIC ANALYSIS

4.1 GENERAL

When subjected to increasing loads of any type, a thin-walled structure will go through three different phases, namely the elastic, the elasto-plastic and the plastic phase. The elastic theory can only predict the behaviour until one of the fibres of the structure begins to yield. In the present case, elastic theory is quite simple, that is, for axial compressive loading Hooke's law is used and for torsional loading the following formula is used.

$$\tau = \frac{T}{2At} \qquad \ldots(3)$$

where τ is the constant shear stress across the profile of constant thickness t, due to a torque T.

and A is the area ($= b^2$) enclosed by the profile.

A non-linear elasto-plastic analysis can be used for the second phase, but it is complicated and expensive in computer time. The final post-collapse behaviour can be analysed using the rigid-plastic theory. This simple, but approximate analysis, is used to ascertain the suddenness of collapse of structures. Basic concepts of rigid-plastic analysis of thin-walled structures and many examples of applications are given by Murray[15]. Rigid-plastic analysis of thin-walled structures is based upon the type and sizes of some local plastic mechanisms observed in the laboratory tests. In the present experiments, different types of complicated local plastic mechanisms were observed (Section 3), but the rigid-plastic analysis is based on the simplified geometry of such mechanisms. The sides of the box-column are considered to deform with identical mechanisms of a constant idealized geometry and therefore only one plate element of the square box-column is considered in the analysis.

4.2 REDUCED PLASTIC MOMENT CAPACITY OF HINGES

The complicated spatial mechanisms are, in fact, formed by means of a consistent arrangement of many straight or curved line hinges (yield lines). In order to analyse the spatial mechanism, one should know the plastic moment capacity of the line hinges. In the case of a simple line hinge with only the axial load acting perpendicular to the hinge, the plastic moment capacity M_p' per unit length is given by[16],

$$M_p' = M_p \left[1 - \left(\frac{\sigma}{\sigma_f}\right)^2\right] \qquad \ldots(4)$$

where $\frac{\sigma}{\sigma_f}$ is the ratio of average axial stress to yield stress

and M_p is the full plastic moment capacity in pure bending

per unit width of plate $\left(=\sigma_f \frac{t^2}{4}\right)$

When the line hinge is inclined to the axial load and the rigid-plastic analysis is carried out using an equilibrium method, Murray[17,18] has shown that it requires a new moment capacity M_p'' per unit width of plate which is given by

$$M_p'' = M_p' \sec^2 (90-\alpha) \qquad \ldots(5)$$

where α is the angle of inclination of line hinge with the axial load. However, when the structure is subjected to combined loads and the hinge is not perpendicular to the line of action of the axial load, no such simple formula is available. In this section the reduced plastic moment capacity of such a hinge is derived by using a von Mises criterion.

Fig.8 shows the plate which carries an average compressive stress σ and an average shear stress τ. The plastic hinge is inclined at an angle α to the line of action of σ. The average compressive stress σ_1 acting normal to the plane of the hinge, the average compressive stress σ_2 acting in the direction of the hinge and the average shear stress τ_{12} associated with them may be found by using Mohr's circle. Thus,

$$\sigma_1 = \frac{\sigma}{2} - \sqrt{\left(\frac{\sigma}{2}\right)^2 + \tau^2}\cos(2\alpha+\beta) \qquad \ldots(6)$$

$$\sigma_2 = \frac{\sigma}{2} + \sqrt{\left(\frac{\sigma}{2}\right)^2 + \tau^2}\cos(2\alpha+\beta) \qquad \ldots(7)$$

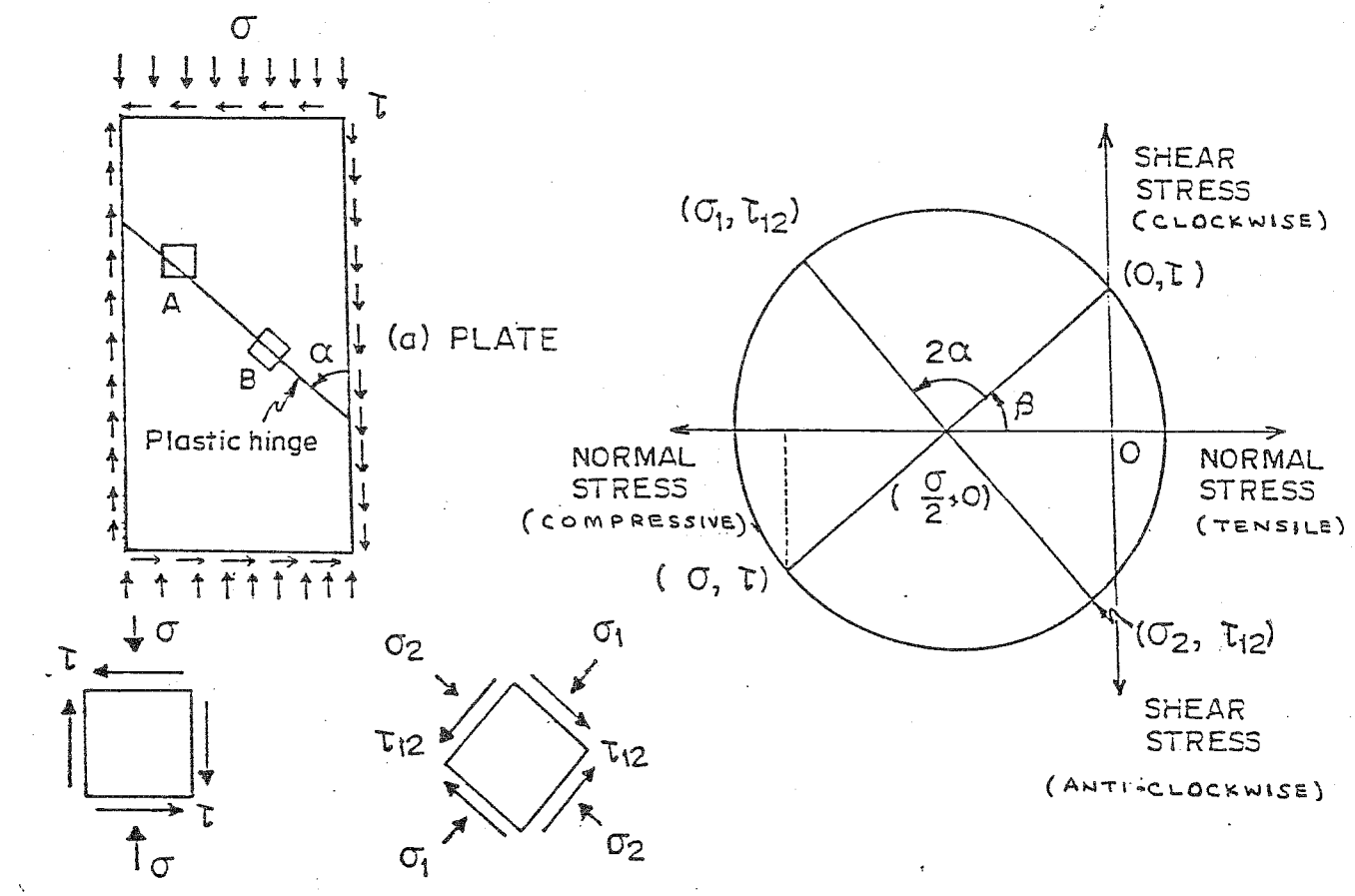

FIGURE 8 Mohr's circle of Stress to determine σ_1, σ_2 and τ_{12}

$$\tau_{12} = \sqrt{\left(\frac{\sigma}{2}\right)^2 + \tau^2}\ \sin(2\alpha+\beta) \qquad \ldots(8)$$

$$\beta = \tan^{-1}\left(\frac{2\tau}{\sigma}\right) \qquad \ldots(9)$$

It must be emphasised that σ_1 is an average compressive stress at the hinge, but there will be a tension yield zone of depth $\frac{t}{2}$ -d and a compression yield zone of depth $\frac{t}{2}$ +d (Fig.9) in which the stresses normal to the hinge plane are σ_{1T} and σ_{1C}, respectively. As in an earlier analysis by Murray[18], it is assumed that the other stresses, viz. σ_2 and τ_{12} are uniformly distributed through the thickness and are therefore given by equations (7) and (8).

Fig.10 shows the distribution of stresses on elements in the compression and tension zones at the hinge face. The von Mises criterion for yielding in these zones gives the following relationships.

(a) for element C

$$\sigma_f^2 = \sigma_{1C}^2 + \sigma_2^2 - \sigma_{1C}\cdot\sigma_2 + 3\tau_{12}^2 \qquad \ldots(10)$$

(b) for element T

$$\sigma_f^2 = \sigma_{1T}^2 + \sigma_2^2 + \sigma_{1T}\cdot\sigma_2 + 3\tau_{12}^2 \qquad \ldots(11)$$

Solving these quadratic equations and letting

$$\sigma_{1C} = k_{1C}\cdot\sigma_f \quad \text{and} \quad \sigma_{1T} = k_{1T}\cdot\sigma_f \qquad \ldots(12)$$

we obtain

$$k_{1C} = R + \frac{\sigma_2}{2\sigma_f} \quad \text{and} \quad k_{1T} = R - \frac{\sigma_2}{2\sigma_f} \qquad \ldots(13)$$

where

$$R = \sqrt{1 - \frac{3}{4}\left(\frac{\sigma_2}{\sigma_f}\right)^2 - 3\left(\frac{\tau_{12}}{\sigma_f}\right)^2} \qquad \ldots(14)$$

In order to locate the dividing line between the tensile and compressive yield zones, an equilibrium analysis can be carried out using Fig.9. Thus,

$$\sigma_1 t = \sigma_{1C}\left(\frac{t}{2} + d\right) - \sigma_{1T}\left(\frac{t}{2} - d\right) \qquad \ldots(15)$$

From equation (6) and solving,

$$\frac{d}{t} = \frac{1}{2R}\left[\frac{\sigma}{\sigma_f} - \frac{3}{2}\,\frac{\sigma_2}{\sigma_f}\right] \qquad \ldots(16)$$

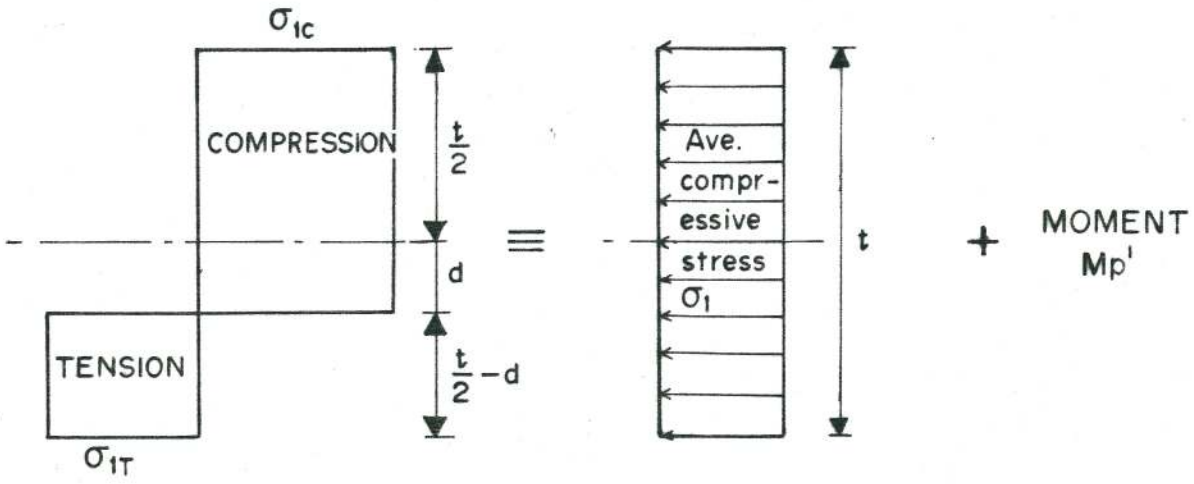
σ_{1c}
COMPRESSION
$\frac{t}{2}$
d
TENSION
$\frac{t}{2}-d$
σ_{1T}
≡
Ave.
compr-
essive
stress
σ_1
t
+
MOMENT
Mp'

Figure 9

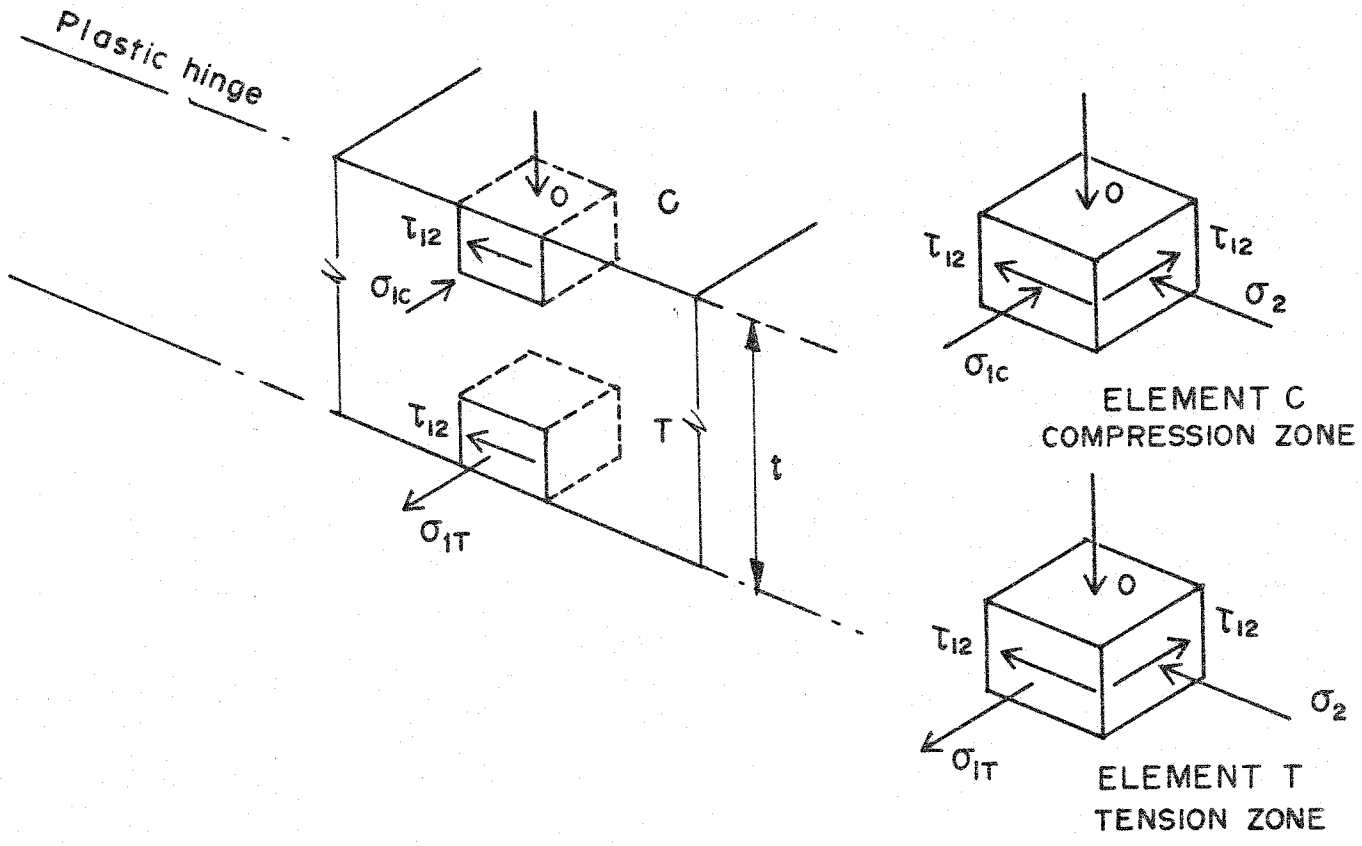
Plastic hinge
O
C
τ_{12}
σ_{1C}
τ_{12}
T
t
σ_{1T}
O
τ_{12}
τ_{12}
σ_2
σ_{1C}
ELEMENT C
COMPRESSION ZONE
O
τ_{12}
τ_{12}
σ_2
σ_{1T}
ELEMENT T
TENSION ZONE

Figure 10

Finally, the plastic moment capacity per unit length of hinge is

$$M_p' = \sigma_{1C}\left(\frac{t}{2}+d\right)\left(\frac{t}{4}-\frac{d}{2}\right) + \sigma_{1T}\left(\frac{t}{2}-d\right)\left(\frac{t}{4}+\frac{d}{2}\right)$$

$$= \frac{\sigma_{1C}+\sigma_{1T}}{2}\left[\left(\frac{t}{2}\right)^2 - d^2\right] \qquad \ldots(17)$$

$$= M_p \cdot R\left[1-\left(\frac{2d}{t}\right)^2\right]$$

This result has been compared with a similar analysis based on the Tresca yield criterion by Mahendran[19].

4.3 RIGID-PLASTIC ANALYSIS OF PLASTIC MECHANISMS OBSERVED IN TESTS WITH AXIAL COMPRESSION ON BOX-COLUMNS

A number of researchers (eg., Murray[20], Walker and Murray[21]) have observed and analysed the roof mechanism for plates of low b/t ratio. However, there were differences in the way they idealized the geometry of the mechanism. Fig.11 shows the idealized roof mechanism in this analysis. Present experiments revealed that the angle α and the ratio r ($=\frac{d_2}{d_1}$) are about 30^o and 0.6, respectively, which are different from those assumed by Murray[20]. As pointed out by Murray[15], any complicated plastic mechanism can be analysed by sub-dividing it into many so-called basic mechanisms. In the present case the mechanism can be considered in two parts, the inner region of width b-2c and the two identical edge regions each of width c, by analysing the equilibrium of a strip element from each region.

For small deflections, this mechanism behaves like a true mechanism since the regions adjoining the mechanism can undergo elastic deformations. Beyond small deflections, the edge regions EAC and FBD wil be yielding to maintain a kinematically admissible mechanism. Therefore at large deflections, the mechanism behaves like a quasi-mechanism[15] formed when a true mechanism (inner region) is combined with yielding regions (edge regions). In this section the large-deflection theory is used to derive the unloading curves.

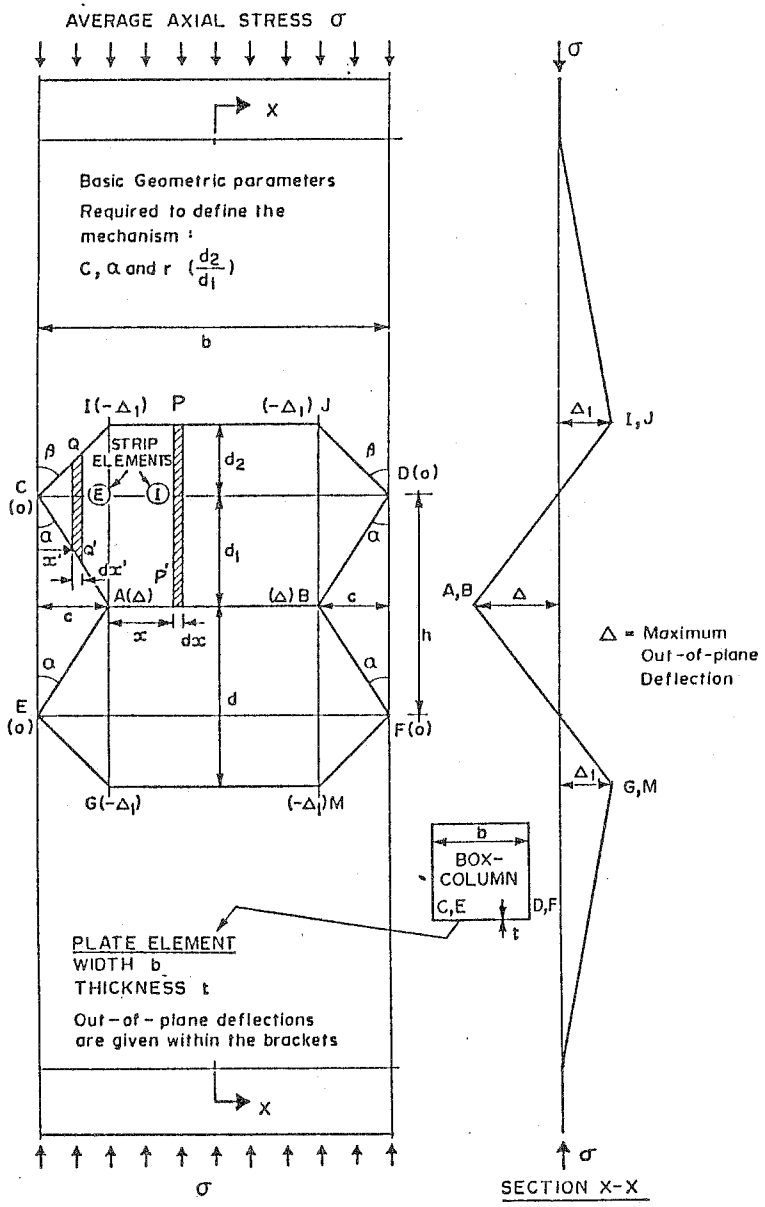

FIGURE 11 Idealized Roof Mechanism for Pure Axial Compression

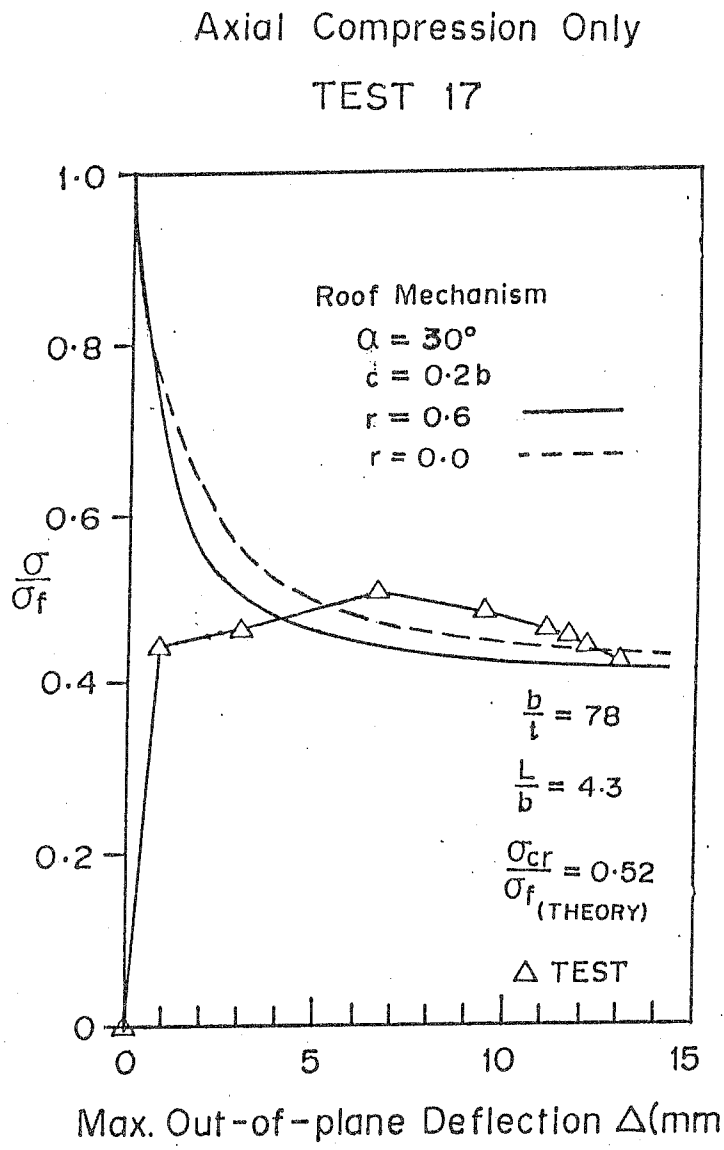

FIGURE 12 Comparison of Theoretical Rigid-plastic Curves and Experimental Results

For the inner region, the hinges are perpendicular to the axial load and thus the M_p' expressions given by equations (4) and (17) are identical. Using the expression for M_p' given by the equation (4) for the equilibrium of the strip element in a similar way to Murray[20], the total force carried by the inner region is obtained.

$$F_{inner} = \sigma_f (b-2c)t \left[\sqrt{(1+r)^2 \left(\frac{\Delta}{t}\right)^2 + 1} - (1+r)\frac{\Delta}{t}\right] \quad ....(18)$$

For the edge regions in large deflections, the force carried by the edge regions is given by

$$F_{edge} = 2\sigma_f ct \quad ...(19)$$

From equations (18) and (19), the average axial stress σ across the box-column is obtained.

$$\frac{\sigma}{\sigma_f} = \frac{b-2c}{b}\left[\sqrt{(1+r)^2 \left(\frac{\Delta}{t}\right)^2 + 1} - (1+r)\frac{\Delta}{t}\right] + \frac{2c}{b} \quad ...(20)$$

Fig.12 compares the theoretical large deflection unloading curves with those of experiments. During testing with all cases of loading, it was observed that the outer hinges tended to move towards the central hinge during large deflections, i.e., r tended to zero. Hence the unloading curve for the geometry of mechanism with r equal to zero, as assumed by Walker and Murray[21], is also plotted in the same figure. Thus the theoretical and experimental results for the roof mechanisms appear to agree reasonably well. The flip-disc mechanism (Fig.13) has also been analysed[19] using four assumed shapes. The analysis is complicated by the presence of kinks at the corners. These kinks allow axial shortening of the specimens to occur.

4.4 RIGID-PLASTIC ANALYSIS OF PLASTIC MECHANISMS OBSERVED IN TESTS WITH LOADS ASSOCIATED WITH TORSION

Fig.14 shows the idealized roof mechanism in this case. The stresses due to these loadings are the torsional shear stress τ and an average axial compressive stress σ_a as shown in the same figure. Each plate element undergoes a shear-type deformation and shortening in its own plane and a

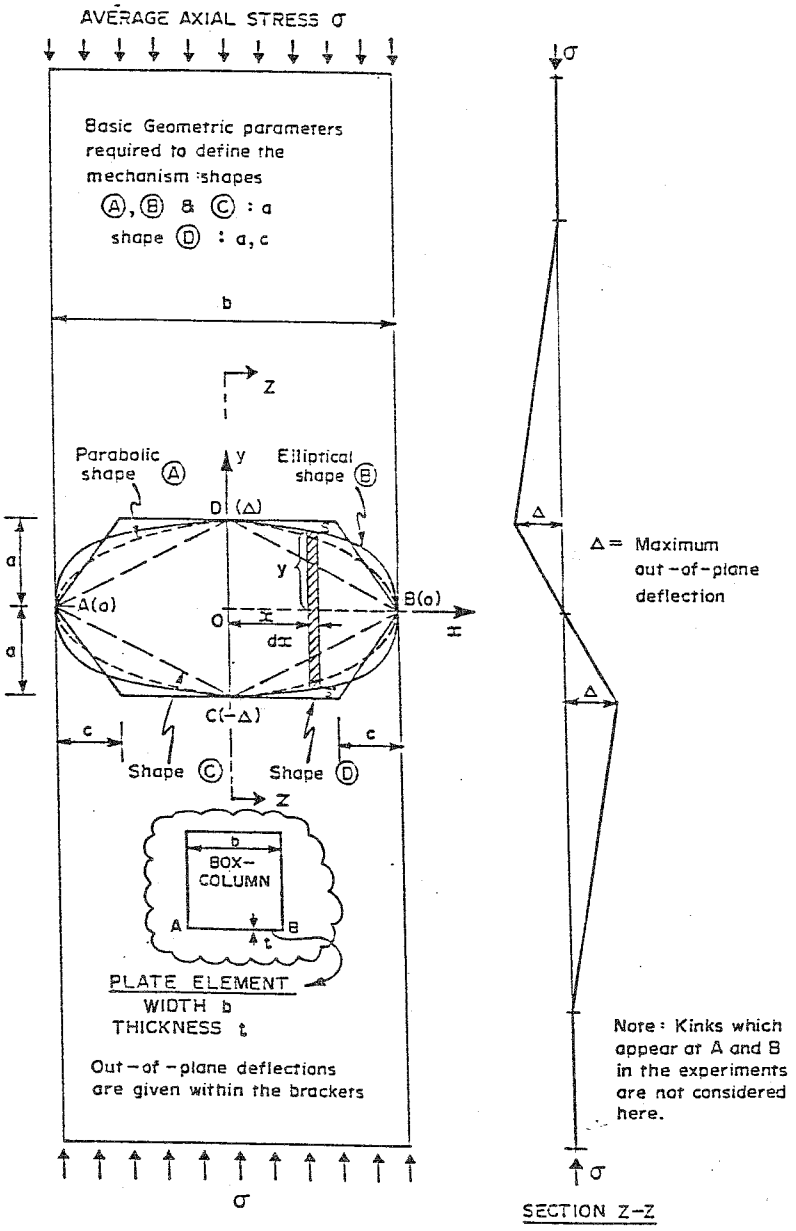

FIGURE 13 Idealized Flip-disc Mechanism for Pure Axial Compression

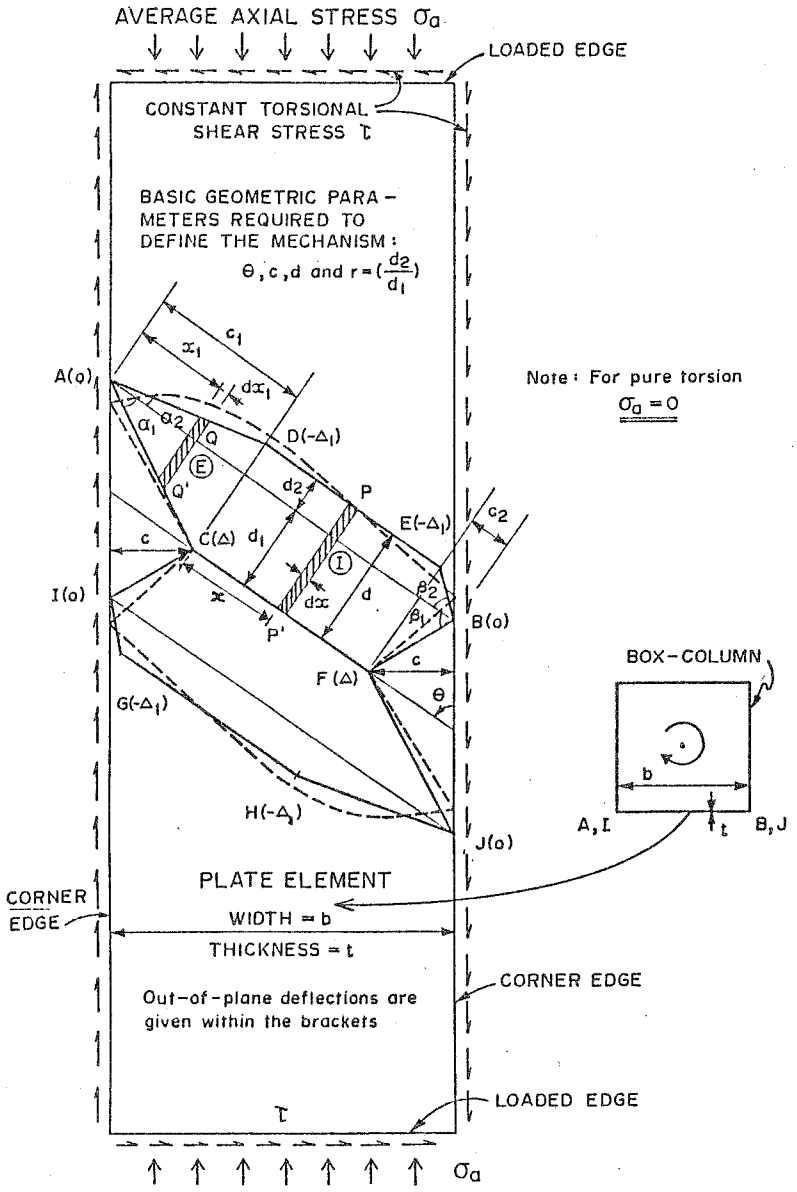

FIGURE 14 Idealized Roof Mechanism for loadings of Combined Axial Compression and Torsion and Pure Torsion

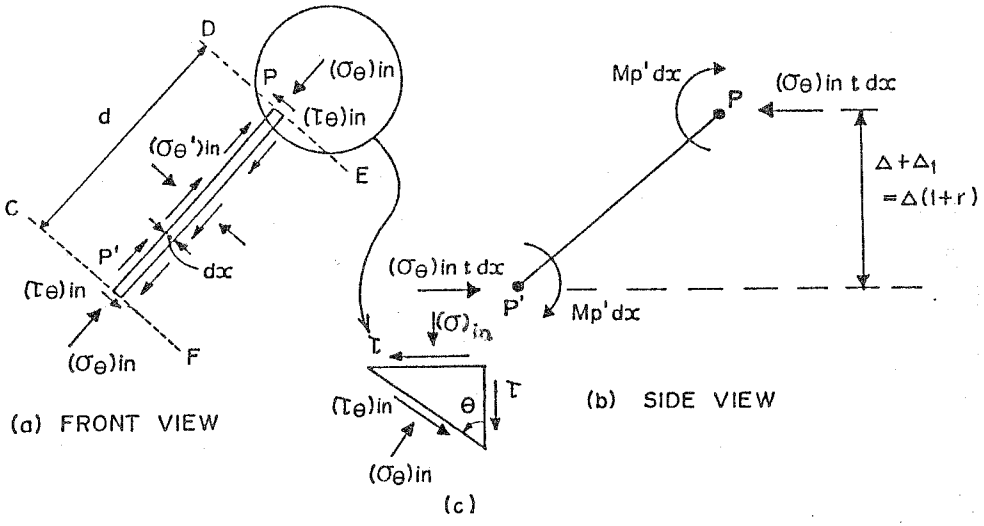

FIGURE 15 A Strip Element in the Inner Region of Roof Mechanism - Torsional Loadings

twisting-type deformation. The twisting-type deformation of plate elements is considered not to affect the out-of-plane deflection. In fact, such twisting-type deformations of plate elements tend to change the shape of the mechanism to that shown by dotted lines in Fig.14. The change of shape of the mechanism becomes less noticeable as the axial compression component in combined loading is increased. For the sake of simplicity, the changes to the shape of the mechanism are ignored in the analysis. Hence the mechanism can be considered to consist of the inner region with parallel hinges and the two edge regions with inclined hinges and again these regions are analysed separately using a large-deflection theory.

We consider a strip element in the inner region with the forces acting on it as shown in Fig.15. As the hinges are inclined at an angle θ to the plate edge parallel to the box-column axis, the stresses are provided with a subscript θ. The shear stress τ acting on a plane parallel to the loaded edge of the plate is assumed to be constant across the box-column at any stage of the loading. It can be shown by considering longitudinal equilibrium of elements around the profile that this assumption will not lead to significant errors. But the associated normal stress σ varies across the width of each plate element with an average axial stress equal to the applied axial stress σ_a, that is,

$$\frac{\sigma_a}{\sigma_f} = \left(1 - \frac{2c}{b}\right) \frac{(\sigma)_{in}}{\sigma_f} + \frac{2c}{b} \frac{(\sigma)_{edge}}{\sigma_f} \qquad \ldots(21)$$

where appropriate additional subscripts are provided to separate the stresses across the regions.

It is to be noted that $(\sigma)_{edge}$ is an average stress across the edge regions whereas $(\sigma)_{in}$ is constant across the inner region.

For rotational equilibrium of the strip element,

$$(\sigma_\theta)_{in} \quad tdx \quad (1+r)\,\Delta = 2\,M_p'\,.dx \qquad \ldots(22)$$

where M_p' is a function of $(\sigma)_{in}$, τ and θ, and is given by equation (17).

Letting $M_p' = R_m . M_p$, we obtain,

$$\frac{(\sigma_\theta)_{in}}{\sigma_f} = \frac{0.5\, R_m}{(1+r)\,\frac{\Delta}{t}} \qquad \ldots(23)$$

The relationship between $(\sigma)_{in}, \tau$ and $(\sigma_\theta)_{in}$ is given by the equations (6) to (9), written in another form, i.e.,

$$(\sigma_\theta)_{in} = (\sigma)_{in} \sin^2\theta + \tau \sin 2\theta \qquad \ldots(24)$$

For large deflections, the edge regions ACI and BFJ are assumed to be yielding under the combined action of shear and axial compression to maintain a kinematically admissible mechanism. Under such conditions, the average stress $(\sigma)_{edge}$ acting on a plane parallel to the loaded edge within the edge regions is given by the following equation.

$$\frac{(\sigma)_{edge}}{\sigma_f} = \sqrt{1 - \left(\frac{\tau}{\tau_f}\right)^2} \qquad \ldots(25)$$

The main aim of this analysis is to obtain values of Δ for various load levels of τ and a constant σ_a. Hence for values of $\frac{\tau}{\tau_f}$ ranging from 0 to 1, $(\sigma)_{edge}$, $(\sigma)_{in}$ and $(\sigma_\theta)_{in}$ are calculated first using equations (25), (21) and (24), respectively, and thus Δ is determined finally from equation (23). This process is repeated for all combinations of torsion and axial compression by using the geometrical parameters of the observed mechanism in each case.

For small deflections, equations similar to (23) are obtained for each edge region by considering the rotational equilibrium of a strip element. These equilibrium equations have to be solved iteratively to satisfy equation (21). The details of this iterative procedure is given by Mahendran[19].

Fig.16 compares the theoretical large-deflection unloading curves derived for the observed value of r and also for r=0 as in the case of axial compression. The agreement is generally good considering the complexity of the mechanism and it improves as the axial compression component in combined

loading increases due to the fact that the idealized mechanism used in the analysis represents more accurately the experimentally observed mechanism in this case than in the case with pure torsion. Theoretical curves confirm the sudden collapse observed for a very large axial compression component in combined loading during testing.

The analysis of flip-disc mechanism (Fig.17) follows that of roof mechanism for small deflections. Since the effect of kinking during large deflections is not accounted for, theoretical curves are found to be underestimated[19]. However, these curves predict the general trend of collapse as the interaction of torsion and axial compression takes place.

5. CONCLUSIONS

This paper presents the details of an experimental programme studying the behaviour of box-columns under various combinations of torsion and axial compression. Experimental interaction diagrams obtained thus can be used in the design of box-columns under these loadings. The use of plate girder ~~girder~~ theories in estimating the ultimate strength of box-columns in torsion is mostly found to be unsafe as observed by Scheer and Nölke[1]. Two types of local plastic mechanisms, namely the roof and flip-disc mechanisms were observed in all cases of loading. Collapse behaviour of these box-columns was studied by means of a simplified rigid-plastic analysis of the observed complicated plastic mechanisms and the results are compared with those of experiments. Large-deflection theoretical curves derived in the case of roof mechanisms agree reasonably well with experimental curves for all cases of loading.

ACKNOWLEDGEMENTS

M.Mahendran would like to thank Monash University for making available the Monash Graduate Scholarship during this research work.

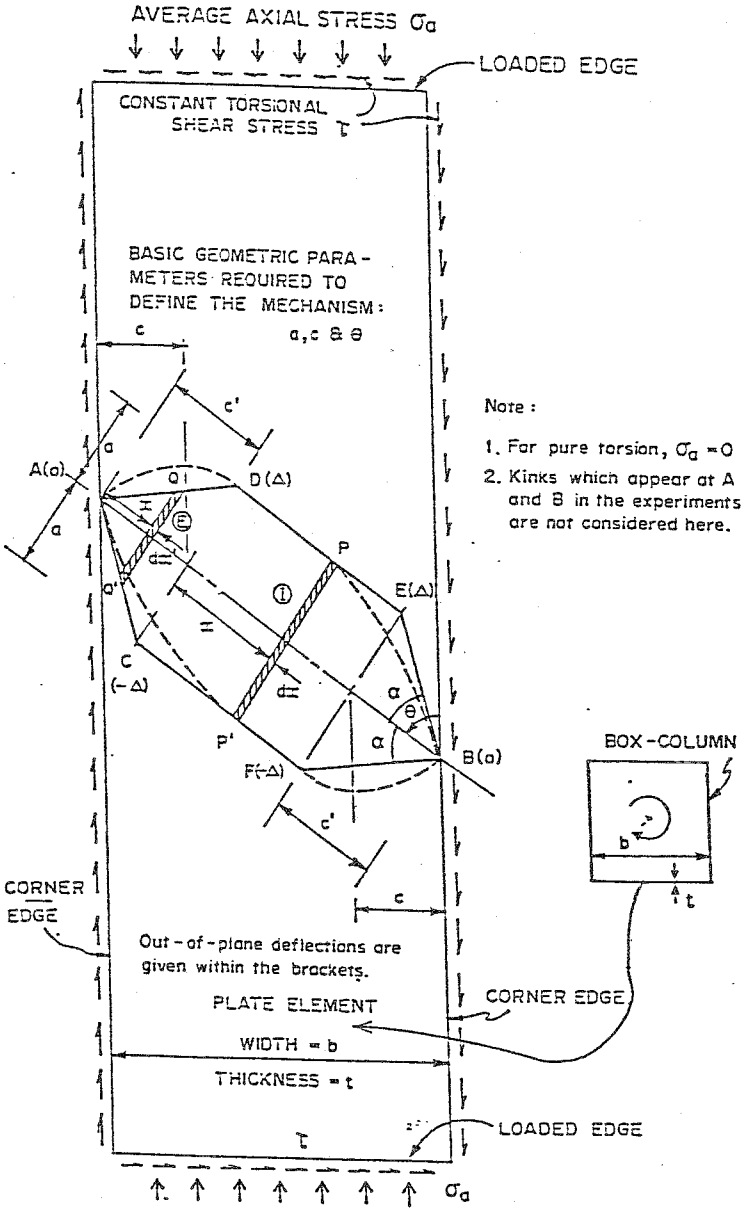

FIGURE 17 Idealized Flip-disc Mechanism for Loadings of Combined Axial Compression and Torsion and Pure Torsion

REFERENCES

1 Scheer,J. and Nölke,H., Traglastversuche an torsionsbelasteten, dunnwandigen Kastentragermodellen, Bauingenieur, 51 (1976) 381-386.

2 DASt Richtlinie 012 - Beulsicherheitsnachweise fur platten, Deutscher Ausehuss fur Stahlbau, Oct 1978.

3 Scheer,J., Nölke,H. and Böhm,M., Traglastversuche an dunnwandigen Kastentragermodellen mit Biegemomentenbeanspruchung, Bauingenieur, 53 (1978) 379-386.

4 Lacher,G. and Böhm,M., Traglastversuche an dunnwandigen Kastentragermodellen mit kombinierter Biegemomenten-und Torsionsbeanspruchung, Bauingenieur, 56 (1981) 45-54.

5 AASHTO, Standard specifications for highway bridges, Eleventh Edition, Washington,D.C., 1977.

6 ECCS, European recommendations for steel construction, The Construction Press, England, 1981.

7 Murray,N.W. and Lau,Y.C., The behaviour of a channel cantilever under combined bending and torsional loads, Thin-walled Structures, 1 (1983) 55-74.

8 Basler,K., Strength of plate girders in shear, J. of the Struct. Div., Proc. ASCE, No.ST7 (Oct 1961) 151-150.

9 Höglund,T., Livets Verkningssatt Och Barformaga Hos Tunnavaggig I-Balk, The Div. of Building Statics and Structural Engineering, The Royal Inst. of Tech., Bulletin Nr.93 (1971), Stockholm.

10 Herzog,M., Die Traglast unversteifter und versteifter, dunnwandiger Blechtrager unter reinem Schub und Schub mit Biegung nach Versuchen, Der Bauingenieur 49 (1974) 382-389.

11 Harding,J.E., Hobbs,R.E. and Neal,B.G., Ultimate load behaviour of plates under combined direct and shear in-plane loading, Steel plated structures, Crosby Lockwood Staples, ed. Dowling,P.J. et al., 1977, 369-403.

12 Dowling,P.J., Frieze,P.A. and Harding,J.E., Imperfection sensitivity of steel plates under complex edge loading, ECCS-IABSE Colloquium on Stability of Steel Structures, Prelim. Report, Liege, April 1977, 305-314.

13 Massonnet,Ch. and Janss,J., A state of art report on tolerances in steel plated structures, The design of steel bridges, ed. Rockey,K.C. and Evans,H.R., Granada, London, 1981, 83-118.

14 Mahendran,M. and Murray,N.W., Elastic buckling analysis of ideal thin-walled structures under combined loading using a finite strip method, Submitted for Publication in Thin-walled Structures.

15 Murray,N.W., Introduction to the theory of thin-walled structures, Oxford Press, London, May 1984.

16 **Matheson,J.A.L., Hyperstatic structures**, Vol.1, Butterworths, London, 1959.

17 **Murray,N.W.**, Das aufnehmbare Moment in einem zur Richtung der Normalkraft schrag liegenden plastischen Gelenk, **Die Bautechnik, 50** (2) (1973) 57-58.

18 **Murray,N.W.**, The effect of shear and normal stresses on the plastic moment capacity of inclined hinges in thin-walled steel structures, **Festschrift Roik, Inst. fur Konstruktiren Ingenieurbau, Rhur Uni Bochum**, Mitt.Nr 84-3 (Sept 1984) 237-248.

19 **Mahendran,M., Box-columns with combined axial compressive and torsional loading**, Ph.D. Thesis, Monash University, June 1985.

20 **Murray,N.W.**, Buckling of stiffened panels loaded axially and in bending, **The Structural Engineer, 51** (8) (Aug 1973) 285-301.

21 **Walker,A.C. and Murray,N.W.**, A plastic collapse mechanism for compressed plates, **Publs. IABSE, 35-I** (1975) 217-236.